ROYAL SOCIETY OF CHEMISTRY

EDGE ARTICLE

Check for updates

Acid–base responsive multifunctional poly(formyl sulfide)s through a facile catalyst-free click polymerization of aldehyde-activated internal diynes and dithiols†

Baixue Li,[a] Xue Wang,[a] Die Huang,[b] Mingzhao Li,[b] Anjun Qin, [ID] *[b] Yusheng Qin [ID] *[a] and Ben Zhong Tang[c]

Acid–base equilibria play a critical role in biological processes and environmental systems. The development of innovative fluorescent polymeric materials to monitor acid–base equilibria is highly desirable. Herein, a novel catalyst-free click polymerization of aldehyde-activated internal diynes and dithiols was established, and exclusively Markovnikov poly(formyl sulfide)s (PFSs) with high molecular weights and moderate stereoregularity were produced in high yields. Because of the aromatic units and sulfur atoms in their main chains, these polymers possessed high refractive index values. By introducing the fluorene and aldehyde moieties, the resulting PFSs could act as a fluorescent sensor for sensitive hydrazine detection. Taking advantage of the reaction of the aldehyde group and hydrazine, imino-PFSs with remarkable and reversible fluorescence change through alternating fumigation with HCl and NH$_3$ were easily acquired and further applied in multicolor patterning, a rewritable material and quadruple-mode information encryption. Additionally, a test strip of protonated imino-polymer for the tracking of bioamines *in situ* generated from marine product spoilage was also demonstrated. Collectively, this work not only provides a powerful click polymerization to enrich the multiplicity of sulfur-containing materials, but also opens up enormous opportunities for these functional polysulfides in diverse applications.

Introduction

In nature, numerous biological creatures, *e.g.*, the chameleon, gray treefrog, octopus, and *Mimosa pudica*, are masters at reversibly changing their colors and shapes in response to the surrounding environment.[1–4] Scientists have made unremitting efforts to construct intelligent artificial materials to mimic natural systems. Stimuli-responsive optical materials with great applications in sensors, anticounterfeiting, information security, smart materials, biotechnology, *etc.*, are a promising approach, as their colours and/or fluorescence properties can be altered sensitively and quickly by external perturbances such as temperature, light, mechanical force, and chemical

[a] College of Chemistry and Chemical Engineering, Yantai University, Yantai 264005, China. E-mail: ysqin@ytu.edu.cn

[b] State Key Laboratory of Luminescent Materials and Devices, Guangdong Provincial Key Laboratory of Luminescence from Molecular Aggregates, Center for Aggregation-Induced Emission, South China University of Technology, Guangzhou 510640, China. E-mail: msqinaj@scut.edu.cn

[c] School of Science and Engineering, Shenzhen Institute of Aggregate Science and Technology, The Chinese University of Hong Kong, Shenzhen (CUHK-Shenzhen), Shenzhen 518172, China

† Electronic supplementary information (ESI) available: Experimental procedures; characterization data of monomers and polymers; and supplemental experimental details. See DOI: https://doi.org/10.1039/d3sc03732k

treatment.[5–10] In view of the particular significance of acid–base homeostasis in physiological and environmental processes, as well as the extraordinary advantages of fluorescence techniques, it is important to exploit new types of smart fluorescent materials for precise monitoring and containment of acid–base states.[11,12]

So far, many acid–base responsive luminescent materials have been explored to achieve this purpose, including, but not limited to, lanthanide complex,[13] inorganic nanocluster,[14] metal–organic framework,[15] hydrogel,[16] quantum dot,[17] molecular and polymer materials.[18–22] Thereinto, major efforts are centered on low-mass fluorophores; polymer-based counterparts, in contrast, show obvious technical superiority, such as excellent processability, facile modification and signal amplification.[23–25] However, the development of acid–base responsive fluorescent polymers is still challenging.

With this in mind, we were motivated to prepare a fluorescent polymeric material with a response to acid–base variation. Typically, imine derivatives originating from the reaction of aldehydes and amines have demonstrated a fast acid–base response in their optical properties owing to the changes in electron distribution during protonation and deprotonation procedures.[26–28] To facilely fabricate polymeric materials, acetylene-based click polymerization is undoubtedly a competitive candidate due to its high
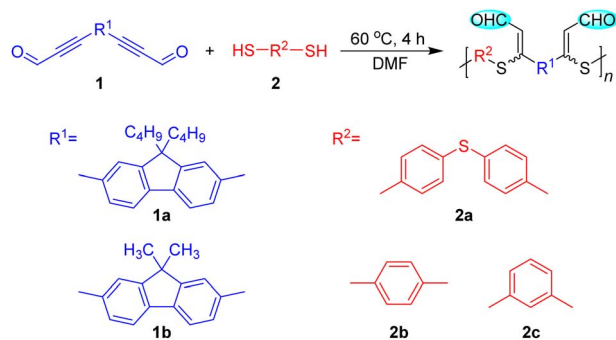
Scheme 1 Catalyst-free click polymerization of aldehyde-activated internal diynes and dithiols.

efficiency and atom economy, great functional group tolerance, and simple product isolation.[29–33] In the context of the "dual carbon" goal, we embarked on our research into the click polymerization of an aldehyde-activated internal alkyne and thiol to achieve a greener and more efficient method to synthesize aldehyde-containing polysulfides.[34–37] More importantly, the deuterogenic imino-polysulfides embedded with luminescence motifs are promising for use as indicators for the illustration of acid–base change.

Herein, a facile catalyst-free click polymerization of aldehyde-activated internal diynes and dithiols was successfully developed, and a series of regio- and stereospecific poly(formyl sulfide)s (PFSs) with satisfactory molecular weights were generated in high yields (Scheme 1). The resultant PFSs possessed high refractive indices, which were ascribed to their high contents of aromatic and sulfur motifs. Fluorene- and aldehyde-containing PFSs could serve as a fluorescent probe for the sensitive and selective detection of hydrazine. It is noteworthy that the imino-PFS derivatives obtained through Schiff base reaction could be protonated and deprotonated reversibly, causing significant color and fluorescence changes during acid–base exposures. Taking advantage of their unique features, the imino-PFSs have a wide range of applications in polychrome photopatterning, rewritable materials, quadruple-mode information encryption and marine product spoilage monitoring.

Results and discussion

Click polymerization

In order to establish the catalyst-free polyhydrothiolation for the preparation of PFSs, aldehyde-activated internal diynes 1 were synthesized according to reported procedures (Scheme S1†), whereas dithiols 2 are commercially available. We used diyne 1a and dithiol 2a as model monomers to optimize the polymerization reaction conditions. The feasibility of the polymerization to be carried out in commonly used solvents was first examined (Table S1†), which demonstrated that a polymer with a high weight-average molecular weight (M_w) could be obtained in high yield in dimethylformamide (DMF). The temperature, monomer concentration, and reaction time were then investigated sequentially. The results from the temperature effect test showed that the M_w values and yields of the products were gradually

enhanced with increasing the temperature from 30 to 60 °C. Considering the energy-saving and economic benefits, the temperature was not further increased, and 60 °C was adopted as the optimal temperature (Table S2†). The appropriate monomer concentration was determined to be 0.25 M, affording a polymer with a M_w of 40 260 in 86% yield. Further increasing the monomer concentration induced the formation of an insoluble polymer gel (Table S3†). During the time course experiment, a satisfactory result was obtained at 4 h, indicative of the high efficiency of this polymerization. Further extending the reaction time had no obvious impact on the M_w and yield of the product. Hence, 4 h was preferred as the optimal reaction time (Table S4†).

Under the optimized polymerization conditions, other aldehyde-activated internal diynes and dithiols were applied to test the universality of this polyhydrothiolation and broaden the structural diversity (Table 1). All the polymerizations propagated smoothly and efficiently in a regiospecific and stereoselective fashion, and soluble PFSs with high M_w values (up to

Table 1 Polymerization results of different monomers[a]

Polymer	Monomer	Yield (%)	$M_w{}^b$	PDI[b]	$E/Z{}^c$ (%)
P1a2a[d]	**1a** + **2a**	86	40 260	2.74	36 : 64
P1a2b	**1a** + **2b**	80	42 390	2.64	38 : 62
P1b2a	**1b** + **2a**	84	22 140	1.84	48 : 52
P1b2b	**1b** + **2b**	85	22 100	1.79	47 : 53
P1b2c	**1b** + **2c**	88	10 850	1.93	31 : 69

[a] Carried out in DMF at 60 °C for 4 h under argon at a monomer concentration of 0.25 M, [**1**] = [**2**]. [b] Estimated via gel permeation chromatography using tetrahydrofuran (THF) as an eluant on the basis of a polystyrene calibration; M_w = weight-average molecular weight; PDI = M_w/M_n; M_n = number-average molecular weight. [c] Ratio of E/Z structure in the polymers determined using ^{1}H NMR. [d] Data taken from Table S4, entry 3.

Fig. 1 FT-IR spectra of **1a** (A), **2a** (B), model compound **3** (C) and **P1a2a** (D).

42 390) were generated in high yields (up to 88%), manifesting the robustness and versatility of this polymerization.

To investigate the polymerization mechanism, we performed polymerization in the presence of γ-terpinene, which can serve as a radical trapper. The results were similar to those without γ-terpinene (Table S5†), demonstrating the nucleophilic addition mechanism of this polyhydrothiolation.[37] Furthermore, thermoanalysis results demonstrated that these PFSs possess good thermal resistance, with decomposition temperatures at 5% weight loss ranging from 313 to 325 °C, along with carbonic residues ranging from 53% to 67% (Fig. S1†).

Structural characterization

The structures of the resultant PFSs were characterized using standard spectroscopic techniques. To facilitate the structural characterization of the polymers, model compound **3** was designed and synthesized (Scheme S2†). The ^{1}H NMR spectrum indicated that only Markovnikov product was obtained with *E* and *Z* conformations (Fig. S2†). The FT-IR, ^{1}H and ^{13}C NMR spectra of polymer **P1a2a**, model compound **3**, and the corresponding monomers **1a** and **2a** are given as examples. In the FT-

IR spectra (Fig. 1), the C≡C stretching vibration of **1a** and the –SH stretching vibration of **2a** were observed at 2183 and 2556 cm^{−1}, respectively. These peaks could not be perceived in the spectra of **P1a2a** and **3**. Additionally, the C=O stretching vibration of the aldehyde group of **1a** at 1659 cm^{−1} was shifted to 1663 and 1665 cm^{−1} in the spectra of **3** and **P1a2a**, respectively, which was probably due to the polarization of the C=O bond caused by the electronegativity difference between neighboring moieties, verifying the occurrence of the polymerization. Similar results were observed in the FT-IR spectra of other polymers (Fig. S3–S6†).

More detailed structural information about the polymers could be obtained using NMR spectroscopy. The thiol protons of **2a** resonating at δ 3.45 disappeared in the spectra of **3** and **P1a2a**. The resonance of the aldehyde protons of **1a** at δ 9.46 was shifted to δ 9.26 and 10.32 and to 9.32 and 10.31 in the spectra of **3** and **P1a2a**, respectively, owing to the formation of the isomeric units. Moreover, new peaks at δ 5.80 and 6.63 corresponding to the resonances of the newly formed ethylene protons in the spectrum of **P1a2a** were also observed. The *E/Z* ratio in **P1a2a** could be deduced from their integrals, and was calculated to be 36/64 (Fig. 2). Similarly, the ratios of the *Z*-isomers of the other polymers could also be obtained, which were in the range of 52–69%, providing direct evidence for the regio- and stereoselectivity of the click polymerization.

The ^{13}C NMR spectra further confirmed the success of the polyhydrothiolation. The resonances of the acetylenic carbons of **1a** at δ 89.45 and 95.97 disappeared in the spectra of **3** and **P1a2a**. Additionally, the resonance peak of the aldehyde carbon of **1a** at δ 176.73 was shifted downfield to δ 190.13 and 190.65 and to 189.69 and 190.38 in the spectra of **3** and **P1a2a**, respectively. Moreover, new resonances associated with the olefinic carbons were observed downfield (Fig. S7†). Similar conclusions could be drawn by analysis of the NMR spectra of the other polymers (Fig. S8–15†).

Light refractivity

The presence of aromatic rings and sulfur atoms in PFSs might endow them with high refractive indices (*n*).[38–40] Indeed, thin
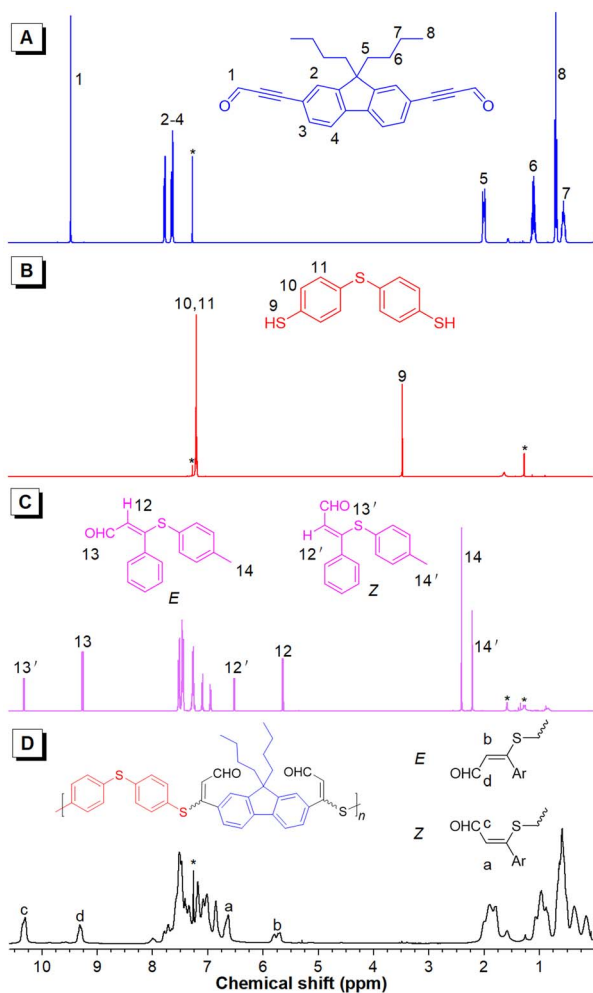

Fig. 2 ^{1}H NMR spectra of **1a** (A), **2a** (B), model compound **3** (C) and **P1a2a** (D) in CDCl₃. The solvent peaks are marked with asterisks.

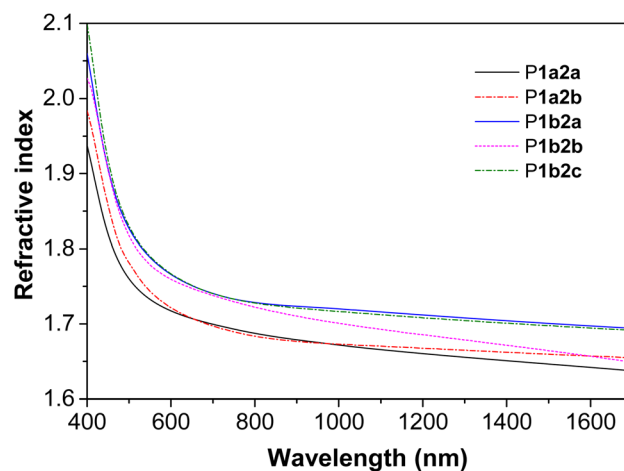**Fig. 3** Wavelength-dependent refractive indices of the thin films of **P1a2a–P1b2c**.

films of **P1a2a**–**P1b2c** with thicknesses ranging from 145.16 to 263.02 nm exhibited n values between 1.637 and 2.099 in a wide spectral region of 400–1700 nm (Fig. 3). Notably, the $n_{632.8}$ values (n values at 632.8 nm) of **P1a2a**, **P1a2b**, **P1b2a**, **P1b2b**, **P1b2c** are 1.710, 1.712, 1.755, 1.751, and 1.756, respectively, which are much higher than those of conventional important optical plastics, such as polycarbonate.[41] Moreover, the Abbe numbers (v_D) and the corresponding chromatic dispersion (D) values of **P1a2a**–**P1b2c** were calculated to be in the ranges of 7.9536–11.1393 and 0.0898–0.1257, respectively (Table S6†). These high refractivity and low chromatic aberration values might enable them to have promising applications in the field of photonic materials.

Hydrazine detection

Taking advantage of the reactive aldehyde group, the fluorene-containing PFSs could serve as a fluorescent probe to sensitively detect hydrazine species, which is important for the natural environment and human health.[42,43] With the addition of hydrazine hydrate to the polymer solution, the absorption of **P1a2a** in the range of 265–330 nm was gradually enhanced, accompanied by an evident color change from colorless to light yellow (Fig. 4A). Additionally, the photoluminescence (PL) intensity of **P1a2a** was increased dramatically with a distinct emission change from almost non-emissive to bright olivine, making it a "turn-on" probe,[44] which might be due to the suppression of nonradiative energy consumption from the C=O bond (Fig. 4B).[45] The quenching

constant (K_{sv}) and the limit of detection (LOD) of **P1a2a** were deduced to be 132 200 M^{-1} and 1.52×10^{-6} M from the Stern–Volmer plots, respectively (Fig. 4C). The specificity of this probe was investigated by measuring the PL response towards various structurally similar analogs. The results showed that only hydrazine induced a dramatic increase in the emission of **P1a2a**, demonstrating the excellent selectivity of this sensor (Fig. 4D).

Acid–base-response-induced optical and photophysical changes

Considering that hydrazine-treated PFS generates imine linkages, their protonation and deprotonation processes might critically regulate the photophysical properties of the polymer. To authenticate this hypothesis and exploit the good film-forming ability of polysulfides, a thin film of imino-**P1a2a** was prepared by drop-coating a mixed solution of **P1a2a** and hydrazine on a quartz plate. The remarkable redshift in the onset absorption wavelength of imino-**P1a2a** changed from 500 to 560 nm after exposure to hydrochloric acid vapor (HCl), triggering a color change from pale yellow to orange (Fig. 5A and Movie S1†). The emission maximum of the PL spectrum shifted from 535 to 645 nm, accompanied with a change in the fluorescence from chartreuse to tangerine (Fig. 5B and Movie S2†). Afterwards, the acid-fumed thin film of imino-**P1a2a** was exposed to ammonia vapor (NH₃), and the absorption and emission of the protonated
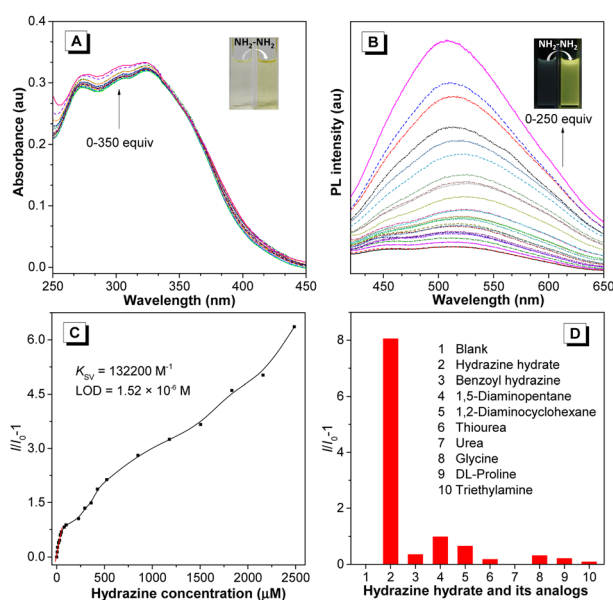

Fig. 4 UV-vis absorption (A) and PL spectra (B) of **P1a2a** *versus* the concentration of hydrazine (0–350 equiv.) in THF solutions. Concentrations: 10^{-5} M, $\lambda_{ex} = 350$ nm. Insets: photographs of the probes before and after the reaction with hydrazine. (C) Plots of $I/I_0 - 1$ of **P1a2a** *versus* hydrazine concentration in THF solutions, where I = peak intensity and I_0 = peak intensity at hydrazine concentration = 0 M. (D) Emission intensity of **P1a2a** at 508 nm in the presence of hydrazine and its analogs (50 equiv. of each), $\lambda_{ex} = 350$ nm.
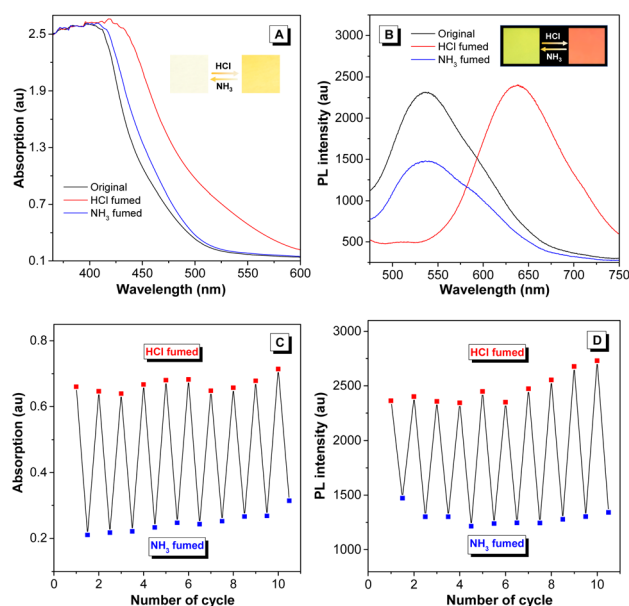

Fig. 5 (A) Absorption spectra and (C) cycling behavior (absorption at 530 nm) of imino–**P1a2a** film from the protonated to the deprotonated form by repeated fuming with HCl and NH₃ vapor. (B) PL spectra and (D) reversible switching of the emission between the jasper (emission at 535 nm) and salmon (emission at 645 nm) states after fuming with HCl vapor followed by NH₃ vapor. Inset photographs show the color and emission changes with the protonation and deprotonation processes.
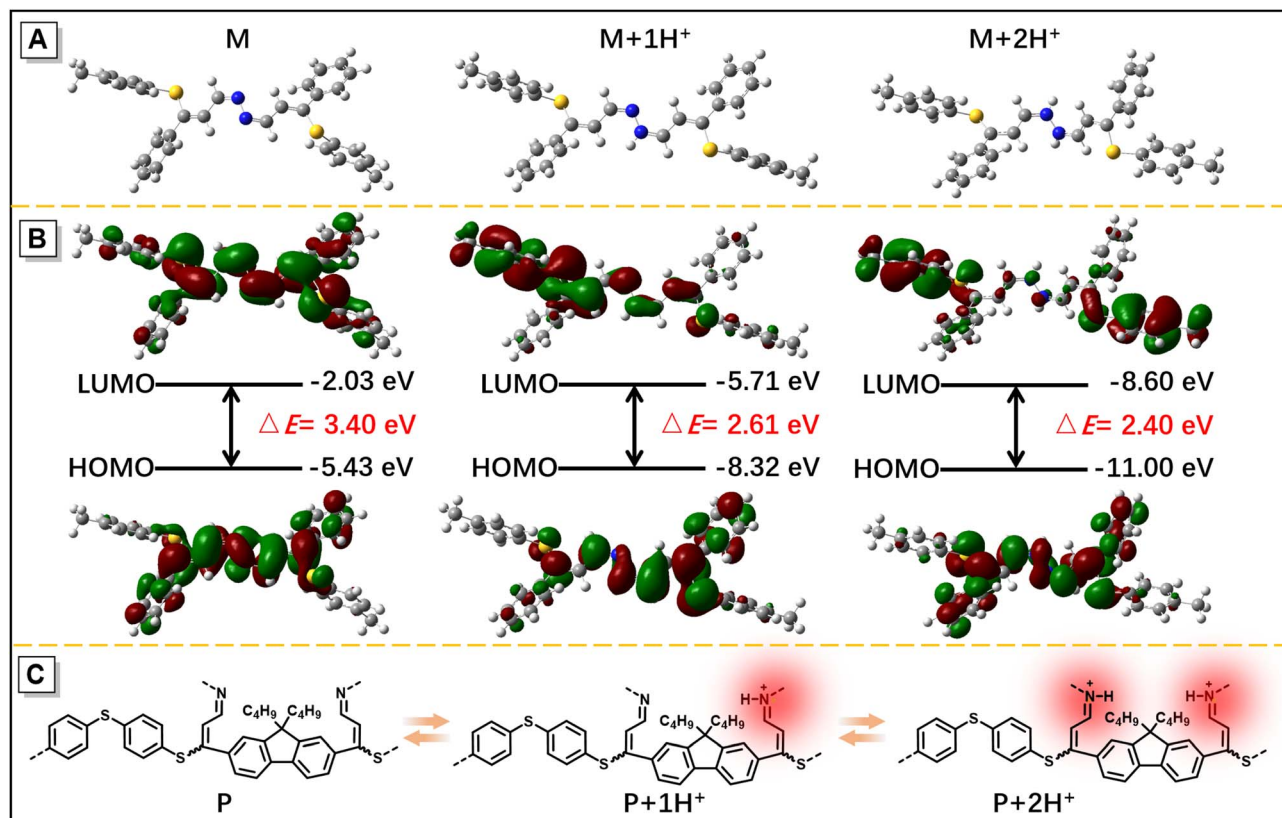
Fig. 6   (A) Optimized structures of M and protonated analogues. (B) Calculated molecular conformation and orbital amplitude plots, along with the energy levels of the HOMOs and LUMOs of M and protonated analogues. (C) Schematic illustration of the acid and amine response mechanism *via* the protonation and deprotonation of imino-P**1a2a**.

thin film were mainly restored to the original positions. We then tested the cycling behavior of the system by alternatively exposing the imino-polymer film to HCl vapor for 5 s and NH_3 vapor for 20 s. The protonated and deprotonated states could be interconverted for at least ten cycles without any apparent decay, suggesting the high reversibility of this response system (Fig. 5C, D and S16†).

To determine the dual-modal sensing mechanism of the imino-polysulfides for HCl and NH_3 vapor, model compound **4** was synthesized, and ^{1}H NMR and FT-IR were used to monitor its protonation and deprotonation processes (Scheme S3†). The resonance of the imine protons of pristine **4** at δ 8.38 exhibited an obvious shift to δ 8.50 after protonation by the addition of trifluoroacetic acid (TFA), while the signals assigned to other resonances remained almost unchanged (Fig. S17†). Moreover, the stretching frequency around 1628 cm^{-1}, which is assigned as the stretching mode of the imine bonds of **4**, was attenuated after exposure to HCl vapor. Simultaneously, a new peak appeared at around 1645 cm^{-1}, which could originate from the newly formed $C=NH^+$ bond (Fig. S18†).[46,47] After deprotonation by the reaction with ammonia, the typical peaks nearly reverted to their initial states, revealing the nondestruction of the molecular structure during the bidirectional changes. These results indicated that the protonation and deprotonation occurred at the imine

nitrogen. To better understand the experimental phenomena, quantum chemical calculations were executed employing the density functional theory (DFT) method at the B3LYP/6-31G(d, p) level. To simplify the calculations, one repeating unit M was used (Fig. S19†). The optimized structures and sketches of the frontier molecular orbitals for M and its protonated states are shown in Fig. 6. Both the highest occupied molecular orbitals (HOMOs) and the lowest unoccupied molecular orbitals (LUMOs) were shifted to lower energies upon protonation, and the estimated energy gaps of the protonated states were narrower than that of the unprotonated one, which was in agreement with the bathochromic absorption of the protonated polymer. In addition, the HOMO and LUMO orbitals of M were mainly concentrated on the C=N and ethenyl bonds, while the absence of the LUMO on the electronegative nitrogen atom of the C=N unit upon protonation demonstrated an evident intramolecular charge transfer feature of the protonated M, which might play a similar role in the redshifted emission of the protonated polymer film. With this insight, the imino-P**1a2a** might exhibit a similar protonated and deprotonated mechanism, as illustrated in Fig. 6C, which represents the redshifted emission of protonated imino-P**1a2a** and its transformation to a blueshifted emissive form by treatment with NH_3.
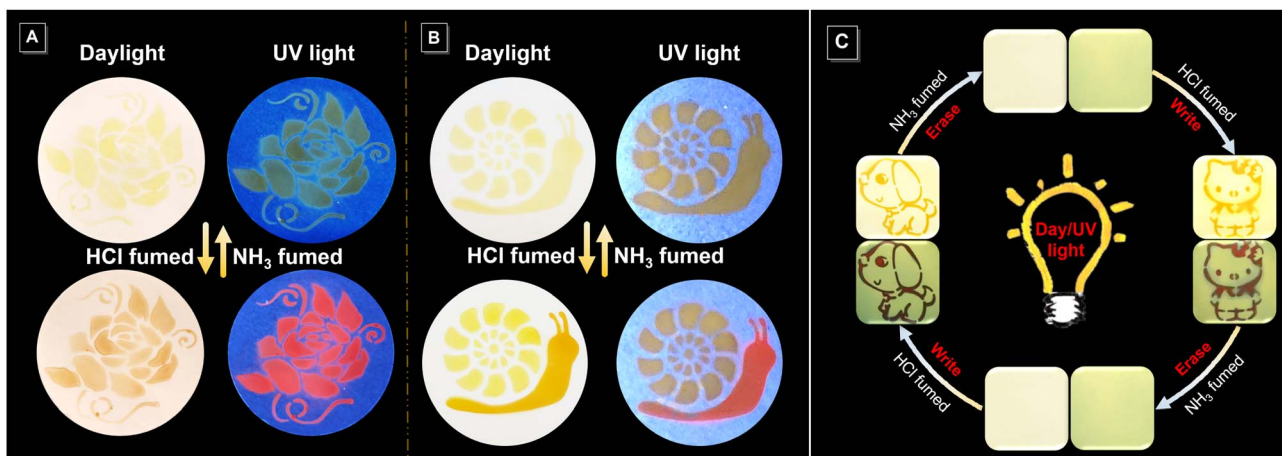
Fig. 7 (A and B) Acid–base responsive patterns achieved by spraying imino-**P1a2a** solution onto filter paper. (C) Schematic illustration of writing and erasing patterns on filter paper using a mask with HCl and NH$_3$ vapor.

Multicolor patterning and rewritable material

Encouraged by its acid–base-responsive color- and emission-switching behavior, we used the imino-polysulfide solution as an ink to draw images on filter paper, which resulted in vivid visible and fluorescent dual-mode colors (Fig. 7A and S20A†). Noticeably, elaborate patterns displaying multiple and gradient colors could also be achieved by tuning the duration of exposure to HCl and NH$_3$ vapor (Fig. 7B and S20B†). Moreover, the rewritable patterning application was also confirmed with the aid of a mask (Fig. 7C). A dog pattern with an orange color under visible light and dark fuchsia fluorescence was obtained by exposing filter paper loaded with imino-**P1a2a** to HCl vapor. The pattern could be quickly erased by treatment with NH$_3$ vapor, and the filter paper was returned to the original state for the next printing. This conceptual demonstration of erasable patterns enables the rapid application of imino-polymers as a medium in the rewritable printing and optical memory fields.

Quadruple-mode information encryption

The integration of imino-polysulfides with unique acid–base responsive feature with additional unresponsive dyes would make them applicable in the information encryption and anti-counterfeiting areas, which are increasingly significant in the current information age (Fig. 8 and S21†).[48–50] An instinctive example to demonstrate this notion is Arabic numerals. Initially, a visible number "8" with yellow fluorescence was painted on a filter paper using imino-**P1a2a** and **P2** (Scheme S4†). Fuming the pattern with HCl vapor led to the appearance of an orange "6" with fuchsia emission, which promptly returned to the pristine state upon treatment with NH$_3$ (Fig. 8A). In addition to digits, imino-**P1a2a** could be applied in a text encryption system. The word "believe" was written; after subsequent fumigation with HCl, the contradictory message "lie" could be clearly recognized. Afterwards, when the letters were treated with NH$_3$, the text quickly recovered to its original

state (Fig. 8B). To further enhance the complexity and diversity, a quadruple-mode information encryption system could be fabricated utilizing a combination of imino-**P1a2a**, MTBZ-Br and **P2** (Scheme S5†). As a proof of concept, the two-color microarray encryption pattern of Code I was constructed, and the encoded information "Activated Internal Alkyne" could be deciphered according to the self-developed algorithm (Fig. 8C and Movie S3†). The magenta and pale-yellow luminescence of Code II was recognized under UV light, and the message "Click Polymerization" could be decoded. Fuming with HCl induced the protonation of imino-**P1a2a**, which triggered a color change from faint yellow to orange, together with an emission transformation from pale-yellow to fuchsia. The specific messages of "Stimuli Responsive" and "Luminescent Material" for Code III and Code IV were read out, respectively. Importantly, the color
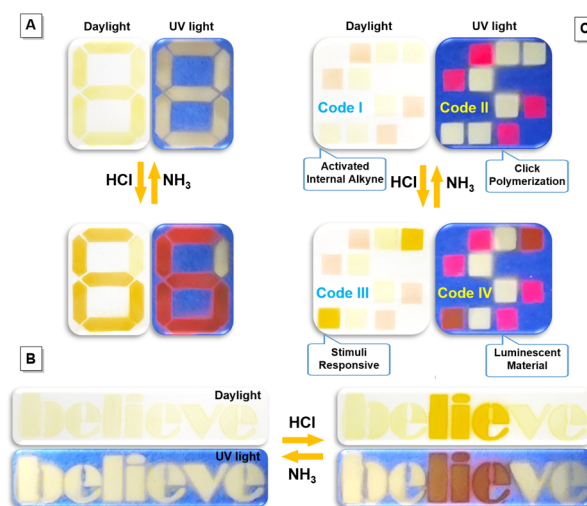

Fig. 8 Photographic images of dual-mode (A and B) and quadruple-mode (C) encryption models achieved by spraying responsive imino-**P1a2a** solution on filter paper. The dialog bubbles reveal the encrypted messages.
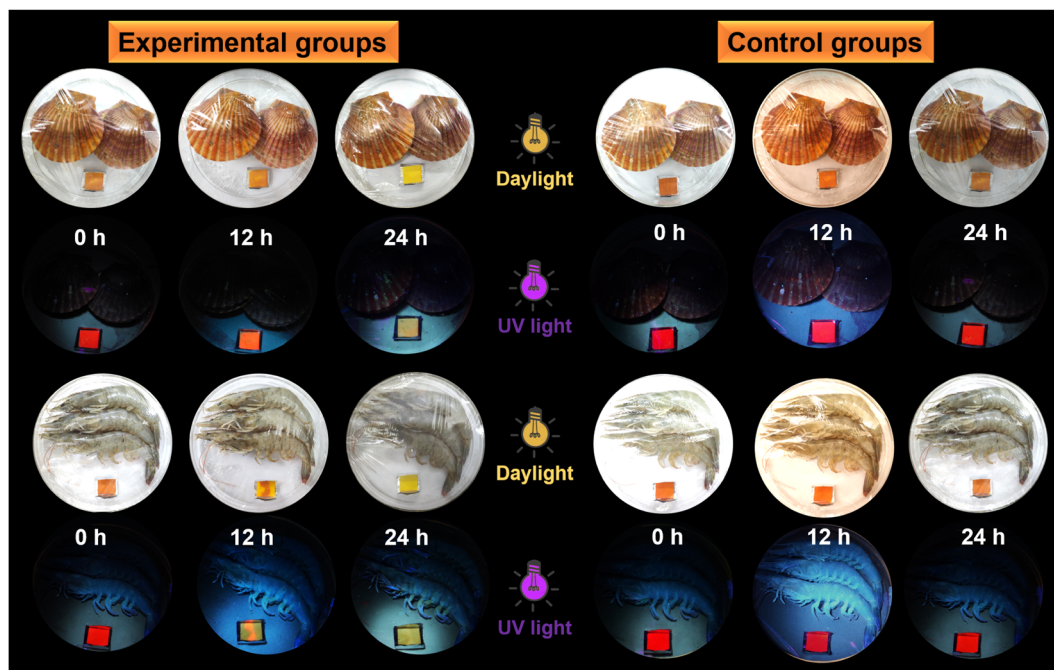
Fig. 9 Spoilage detection of marine products in sealed packages for 24 h at room temperature (experimental groups) and 4 °C (control groups) using protonated imino–P**1a2a** filter paper. Photographs were taken under normal illumination and UV irradiation.

codes could be reconverted by means of NH_3, which enables reversible, multilevel data encryption and decryption, and improves the density of data storage as well as the level of security for the confidential information.

Visualization of seafood spoilage

Taking into consideration that ammonia can induce color and emission changes in the protonated polysulfide, could the biogenic amines generated from the food spoilage process produce similar performance?[51–53] Test strips of protonated imino-P**1a2a** were placed together with fresh scallops, shrimp and silvery pomfret, and kept at room temperature or 4 °C for 24 h to evaluate the spoilage of seafood (Fig. 9 and S22†). Compared to the control groups, the degree of seafood spoilage after storage for 12–24 h increased gradually, and the color of the test strips changed from orange to pale yellow under normal light. Meanwhile, the fluorescence emission varied from fuchsia to jacinth to maize-yellow upon UV irradiation. Hence, the protonated imino-polysulfide could serve as a sensitive sensor to provide a convenient and cost-effective way for monitoring seafood spoilage.

Conclusion

In this work, exclusively Markovnikov adducts of PFSs with high molecular weights and satisfactory yields have been synthesized using a catalyst-free click polymerization of aldehyde-activated internal diynes and dithiols. The high contents of sulfur atoms and aromatic rings endowed the PFSs with high n values. Thanks to the highly reactive

aldehyde units and fluorene moieties in the polymer chains, the PFSs could act as a fluorescent sensor for the selective and sensitive detection of hydrazine. Notably, the resultant imino-PFSs, which were generated from the reaction of aldehyde groups and hydrazine, exhibited attractive acid–base responsive properties, *i.e.*, reversible changes in color and emission during the protonation and deprotonation courses. Based on their unique responsive features, the imino-polymers showed great potential applications in multicolor photopatterning and rewritable materials. Additionally, a quadruple-mode cryptosystem with high storage density and enhanced dimensionality was realized to ensure reliability and security. In addition, protonated imino-PFS as a fluorescent probe for the perception of biogenic amines generated from food spoilage was also constructed in a portable and effective manner. Thus, this work not only provides a facile catalyst-free click polymerization of aldehyde-activated internal diynes and dithiols, but also affords functional PFSs and derivatives with versatile properties and applications.

Data availability

The datasets supporting this article have been uploaded as the ESI.†

Author contributions

B. Li, Y. Qin and A. Qin envisioned the project and designed the experiments. B. Li prepared samples and carried out tests. X. Wang helped analyse DFT calculation results. D. Huang and M.

Li performed refractive index experiment. B. Li, Y. Qin, A. Qin and B. Z. Tang contributed to writing and editing the paper.

Conflicts of interest

There are no conflicts to declare.

Acknowledgements

Notes and references

1 L. C. van Loon, *Trends Plant Sci.*, 2016, **21**, 286–294.
2 D. G. Hamilton, M. J. Whiting and S. R. Pryke, *Behav. Ecol.*, 2013, **24**, 1138–1149.
3 R. C. Duarte, A. A. V. Flores and M. Stevens, *Philos. Trans. R. Soc., B*, 2017, **372**, 20160342.
4 H. N. Skold, S. Aspengren and M. Wallin, *Pigm. Cell Melanoma Res.*, 2013, **26**, 29–38.
5 P. Theato, B. S. Sumerlin, R. K. O'Reilly and T. H. Epps, III, *Chem. Soc. Rev.*, 2013, **42**, 7055–7056.
6 M. Mrinalini and S. Prasanthkumar, *ChemPlusChem*, 2019, **84**, 1103–1121.
7 Q. Yan and S. Wang, *Mater. Chem. Front.*, 2020, **4**, 3153–3175.
8 Y. Yang, J. Yang, M. Fang and Z. Li, *Chem. Res. Chin. Univ.*, 2021, **37**, 598–614.
9 C. H. Wu, P. Q. Nhien, T. T. K. Cuc, B. T. B. Hue and H. C. Lin, *Top. Curr. Chem.*, 2023, **381**, 2.
10 B. Huang, H. Kang, C. W. Zhang, X. L. Zhao, X. Shi and H. B. Yang, *Commun. Chem.*, 2022, **5**, 127.
11 N. A. Masco, *J. Infus. Nurs.*, 2016, **39**, 288–295.
12 M. Wu, K. Li, Y. Liu, K. Yu, Y. Xie, X. Zhou and X. Yu, *Biomaterials*, 2015, **53**, 669–678.
13 D. Zhao, J. Yang, X. Tian, J. Wei, Q. Li and Y. Wang, *Chem. Eng. J.*, 2022, **434**, 134806.
14 K. Yonesato, S. Yamazoe, S. Kikkawa, D. Yokogawa, K. Yamaguchi and K. Suzuki, *Chem. Sci.*, 2022, **13**, 5557–5561.
15 Y. Li, H. Li and Z. Xu, *New J. Chem.*, 2022, **47**, 947–951.
16 M. Vázquez-González and I. Willner, *Angew. Chem., Int. Ed.*, 2020, **59**, 15342–15377.
17 M. Moradi, I. Staude, T. Pertsch, M. Jäger and U. S. Schubert, *Nanoscale*, 2022, **14**, 12395–12402.
18 N. Bar and P. Chowdhury, *ACS Appl. Electron. Mater.*, 2022, **4**, 3749–3771.
19 Z. Li, P. Liu, X. Ji, J. Gong, Y. Hu, W. Wu, X. Wang, H. Q. Peng, R. T. K. Kwok, J. W. Y. Lam, J. Lu and B. Z. Tang, *Adv. Mater.*, 2020, **32**, 1906493.
20 Z. M. Png, C. G. Wang, J. C. C. Yeo, J. J. C. Lee, N. E. Surat'man, Y. L. Tan, H. Liu, P. Wang, B. H. Tan, J. W. Xu, X. J. Loh and Q. Zhu, *Mol. Syst. Des. Eng.*, 2023, **8**, 1097–1129.
21 Y. Hu, T. Han, N. Yan, J. Liu, X. Liu, W. X. Wang, J. W. Y. Lam and B. Z. Tang, *Adv. Funct. Mater.*, 2019, **29**, 1902240.
22 J. Yang, M. Fang and Z. Li, *Acc. Mater. Res.*, 2021, **2**, 644–654.
23 H. N. Kim, Z. Guo, W. Zhu, J. Yoon and H. Tian, *Chem. Soc. Rev.*, 2011, **40**, 79–93.
24 C. Qian, S. Zhu, P. Feng, Y. Chen, J. Yu, X. Tang, Y. Liu and Q. Shen, *ACS Appl. Mater. Interfaces*, 2015, **7**, 18581–18589.
25 B. Song, R. Zhang, R. Hu, X. Chen, D. Liu, J. Guo, X. Xu, A. Qin and B. Z. Tang, *Adv. Sci.*, 2020, **7**, 2000465.
26 H. S. Jung, K. C. Ko, J. H. Lee, S. H. Kim, S. Bhuniya, J. Y. Lee, Y. Kim, S. J. Kim and J. S. Kim, *Inorg. Chem.*, 2010, **49**, 8552–8557.
27 Y. Xie, G. Shan, Z. Zhou and Z. Su, *Sens. Actuators, B*, 2013, **177**, 41–49.
28 F. Wang, T. Qi, Z. Su and Y. Xie, *J. Mol. Model.*, 2018, **24**, 58.
29 A. Qin, J. W. Y. Lam and B. Z. Tang, *Chem. Soc. Rev.*, 2010, **39**, 2522–2544.
30 Y. Liu, A. Qin and B. Z. Tang, *Prog. Polym. Sci.*, 2018, **78**, 92–138.
31 B. He, J. Huang, X. Liu, J. Zhang, J. W. Y. Lam and B. Z. Tang, *Prog. Polym. Sci.*, 2022, **126**, 101503.
32 B. Li, J. Wang, B. He, A. Qin and B. Z. Tang, *Chin. J. Chem.*, 2022, **40**, 2001–2013.
33 X. Fu, A. Qin and B. Z. Tang, *Aggregate*, 2023, e350.
34 R. G. Bass, E. Cooper, P. M. Hergenrother and J. W. Connell, *J. Polym. Sci., Part A: Polym. Chem.*, 1987, **25**, 2395–2407.
35 L. R. Dix, J. R. Ebdon and P. Hodge, *Eur. Polym. J.*, 1995, **31**, 653–658.
36 H. Kuroda, I. Tomita and T. Endo, *Macromolecules*, 1995, **28**, 6020–6025.
37 J. Du, D. Huang, H. Li, A. Qin, B. Z. Tang and Y. Li, *Macromolecules*, 2020, **53**, 4932–4941.
38 J. Liu and M. Ueda, *J. Mater. Chem.*, 2009, **19**, 8907–8919.
39 C. J. Yang and S. A. Jenekhe, *Chem. Mater.*, 1994, **6**, 196–203.
40 J. Zhang, T. Bai, W. Liu, M. Li, Q. Zang, C. Ye, J. Z. Sun, Y. Shi, J. Ling, A. Qin and B. Z. Tang, *Nat. Commun.*, 2023, **14**, 3524.
41 *Refractive index database*, **https://refractiveindex.info/** (accessed: August, 2023).
42 C. A. Reilly and S. D. Aust, *Chem. Res. Toxicol.*, 1997, **10**, 328–334.
43 B. K. Sinha and R. P. Mason, *J. Drug Metab. Toxicol.*, 2014, **5**, 168.
44 Y. Song, L. Zong, L. Zhang and Z. Li, *Sci. China: Chem.*, 2017, **60**, 1596–1601.
45 J. Fan, Y. Zhang, Y. Zhou, L. Lin and C. K. Wang, *J. Phys. Chem. C*, 2018, **122**, 2358–2366.
46 J. Yang, A. Acharjya, M. Y. Ye, J. Rabeah, S. Li, Z. Kochovski, S. Youk, J. Roeser, J. Grgneberg, C. Penschke, M. Schwarze, T. Wang, Y. Lu, R. van de Krol, M. Oschatz, R. Schomacker, P. Saalfrank and A. Thomas, *Angew. Chem., Int. Ed.*, 2021, **60**, 19797–19803.
47 L. Ascherl, E. W. Evans, J. Gorman, S. Orsborne, D. Bessinger, T. Bein, R. H. Friend and F. Auras, *J. Am. Chem. Soc.*, 2019, **141**, 15693–15699.
48 Y. Zhuang, X. Ren, X. Che, S. Liu, W. Huang and Q. Zhao, *Adv. Photonics*, 2021, **3**, 014001.

49 A. Abdollahi, H. Roghani-Mamaqani, B. Razavi and M. Salami-Kalajahi, *ACS Nano*, 2020, **14**, 14417–14492.

50 B. Li, Z. Li, K. You, A. Qin and B. Z. Tang, *Sci. China: Chem.*, 2022, **65**, 771–777.

51 P. Visciano, M. Schirone, R. Tofalo and G. Suzzi, *Front. Microbiol.*, 2012, **3**, 188.

52 Y. J. Diaz, Z. A. Page, A. S. Knight, N. J. Treat, J. R. Hemmer, C. J. Hawker and J. R. de Alaniz, *Chem.–Eur. J.*, 2017, **23**, 3562–3566.

53 M. Papageorgiou, D. Lambropoulou, C. Morrison, E. Modzinska, J. Namiesnik and J. Plotka-Wasylka, *TrAC, Trends Anal. Chem.*, 2018, **98**, 128–142.